Propagation length of mesoscopic photocurrents in a two-dimensional electron gas

Markus Stallhofer,[1] Christoph Kastl,[1] Marcel Brändlein,[1] Christoph Karnetzky,[1] Dieter Schuh,[2] Werner Wegscheider,[3] and Alexander W. Holleitner[1,*]

[1]*Walter Schottky Institut and Physik-Department, Technische Universität München, Am Coulombwall 4a, D-85748 Garching, Germany*

[2]*Institut für Experimentelle und Angewandte Physik, Universität Regensburg, D-93040 Regensburg, Germany*

[3]*Laboratorium für Festkörperphysik, ETH Zürich, Schafmattstrasse 16, 8093 Zürich, Switzerland*

(Received 28 June 2012; published 7 September 2012)

We investigate the average propagation length of photogenerated nonequilibrium electrons in a two-dimensional electron gas using a quantum point contact as a local photocurrent detector. To this end, electrons are photogenerated both quasiresonantly and nonresonantly to the optical interband transition in the quantum well comprising the two-dimensional electron gas. The photocurrent is analyzed as a function of the distance between the excitation spot in the two-dimensional electron gas and the detector. We find that the determined propagation length depends nonmonotonically on the laser intensity. We interpret the observation by an interplay of an enlarged scattering phase space of the photogenerated electrons and the screening of sample specific scatterers.

DOI: 10.1103/PhysRevB.86.115313 PACS number(s): 73.23.−b, 85.35.Be, 85.60.−q, 72.20.Dp

I. INTRODUCTION

The electron-electron scattering of quasiparticles with an excess energy above the Fermi energy of a two-dimensional electron gas (2DEG) has been theoretically described by several groups.[1–5] Such processes preserve the total momentum of the electron system, and in turn, they usually do not contribute directly to the resistance in common transport experiments. In a variety of experiments, Molenkamp and co-workers used one-dimensional quantum point contacts (QPCs) as emitters and detectors for beams of hot electrons and therefore were able to analyze electron-electron scattering and thermoelectric processes in 2DEGs.[6–11] Related work by Schäpers *et al.* revealed the temperature dependence of the electron-electron scattering time,[12] and for large excess energies, Schinner *et al.* focused on the additional electron-phonon interaction in such electron beams.[13,14] Recently, Topinka *et al.* introduced a scanning gate technique[15,16] which allows to spatially resolve the electron-electron scattering in such electron beams in close vicinity of a QPC.[17] Although complementary optical experiments highlighted the relaxation and thermalization dynamics of photogenerated hot electrons in 2DEGs,[18–20] none of the above experiments focused on the impact of charge carrier interaction on photoinduced transport currents in 2DEGs.

Here we present scanning photocurrent measurements performed on low-dimensional electron circuits to explore the average propagation length and hereby the scattering dynamics of photogenerated nonequilibrium charge carriers in a 2DEG. In particular, electron-hole pairs are photogenerated in an AlGaAs/GaAs quantum well comprising a 2DEG, and the resulting current of photogenerated hot electrons in the 2DEG through an adjacent QPC is measured as a function of the laser spot position. The QPC acts as an adjustable energy filter for the photogenerated electrons due to its one-dimensional subbands.[21,22] Therefore, the photocurrent across the QPC shows quantization steps.[23] The described optical beam induced current (OBIC)[24] spectroscopy allows us to spatially resolve and energetically analyze the nonequilibrium flow of photogenerated electrons in the low-dimensional electron circuit, before the photogenerated electrons and holes recombine with each other. Analyzing the exponential decay of the OBIC amplitude as a function of the distance to the QPC, we deduce the average propagation length of the photogenerated electron ensemble in the 2DEG as a function of the photon energy and laser intensity.[23] For both quasiresonant and nonresonant photoexcitation of the optical interband transition from the valence to the conduction band in the quantum well, the extracted propagation length of the photocurrent δ_{decay} depends nonmonotonically on the laser intensity. For low excitation intensities we observe a quasiballistic optoelectronic transport regime in which δ_{decay} approaches the elastic mean free path l_{mfp} of the 2DEG without laser excitation. For intermediate intensities, δ_{decay} decreases. We interpret the decrease to be caused by an enlarged phase space for individual scattering processes such as electron-electron scattering, as more and more electrons are photogenerated. For the highest laser intensities, δ_{decay} increases again, which we explain by a Thomas-Fermi screening of momentum scatterers at an overall increased electron density of the 2DEG including the photogenerated electrons. In this regime, the thermalization of the charge carrier ensemble gives rise to an optically induced quasi-Fermi level which dominates the optoelectronic dynamics in the 2DEG.

We gain further insights into the photogenerated carrier dynamics by analyzing the amplitude of the OBIC A_{OBIC}. For low excitation intensities, A_{OBIC} depends linearly on the laser intensity. This finding is consistent with the interpretation of a quasiballistic optoelectronic transport regime. For a further increasing laser intensity P_{laser}, we observe that A_{OBIC} is proportional to $\sqrt{P_{\mathrm{laser}}}$. By analyzing the energy spectrum of the photocurrent by the help of the QPC, we can exclude a photoinduced thermoelectric current across the QPC to cause the square root dependence. Instead, we can explain it by the existence of the photoinduced quasi-Fermi level in combination with the increasing influence of recombination processes between the photogenerated electrons and holes for the highest laser intensities. Furthermore, we can exclude a dominating influence of plasmons, the second subband of the quantum well, and longitudinal optical phonons on the described

optoelectronic dynamics. Generally, our observations underline the predominant influence of scattering and screening processes on mesoscopic and nanoscale photocurrents and therefore photodetectors.

II. EXPERIMENTAL CIRCUITRY

The QPC is lithographically fabricated in an AlGaAs/GaAs heterostructure. The 2DEG resides in a 25 nm wide GaAs quantum well embedded within AlGaAs tunneling barriers 95 nm below the sample's surface.[25,26] In transport measurements without laser excitation, the mobility, Fermi energy, and the elastic mean free path of the 2DEG are determined to be $\mu = 1.74 \times 10^6$ cm^2/Vs, $E_F = 9.8$ meV, and $l_{mfp} = 15.1$ μm at $T = 4.2$ K. The optical transition energy from the valence to the conduction band of the quantum well including E_F is experimentally determined to be $E_{QW} = 1.543$ eV. A shallow wet etching process is used to define a narrow constriction of approximately 300 nm lithographic width between two etched circles of 15 μm radius.[23,26–28] In combination with a lateral depletion width of ~100 nm, this constriction acts as a one-dimensional QPC in the 2DEG. As sketched in Fig. 1(a), the two 2DEG regions adjacent to the QPC are connected to the voltage source providing the bias voltage V_{SD} and the current voltage amplifier, respectively. An opaque gold gate on top of the QPC is connected to a gate voltage V_G which serves to adjust the one-dimensional subbands of the QPC with respect to the Fermi energy of the 2DEG.

The mesoscopic circuit is placed in the focus of a confocal optical free beam microscope in a helium bath cryostat at a temperature of $T = 4.2$ K. Due to diffraction, the measured spatial resolution of our setup is 1−2 μm. Thermal radiation causes the sample lattice temperature to rise to about 8 − 10 K. The photon energy is varied between $E_{ph,1} = 1.546$ eV (quasiresonant excitation of the optical interband transition of the quantum well) and $E_{ph,2} = 1.598$ eV (nonresonant excitation). The energetic FWHM of the lasers is ~8 meV. The excess energy of electrons above the Fermi edge at the carrier generation spot is defined as $\Delta E = E_{ph} - E_g^* - E_F - E_h$, with E_g^* the effective band gap in the quantum well and E_h the energy portion transferred to the photogenerated hole in the valence band. Considering the electron and hole masses, $E_{ph,2}$ corresponds to an electronic excess energy $\Delta E = 49$ meV above E_F of the 2DEG. We laterally scan the focus spot of a pulsed semiconductor laser with respect to the QPC and simultaneously detect A_{OBIC} across the QPC. Most importantly, we utilize a fast lock-in amplifier triggered to the laser repetition frequency of $f_{trigger} = 40$ MHz. The underlying reason for such a high frequency is that the potential landscape of the low-dimensional QPC-based circuit favors a drift of the photogenerated holes towards the location of the QPC below the opaque topgate. Therefore, they are spatially separated from the photogenerated electrons, and they alter the conductance across the QPC by a dynamic photoconductive gain effect. We determine the dynamics due to the photogenerated holes to occur in the order of milliseconds, as discussed in detail in Ref. 26. Such slow processes act only as a quasistatic background to the OBIC at 40 MHz, and the signal is dominated by much faster processes induced by the photogenerated electrons.[23] Because of the large impedance

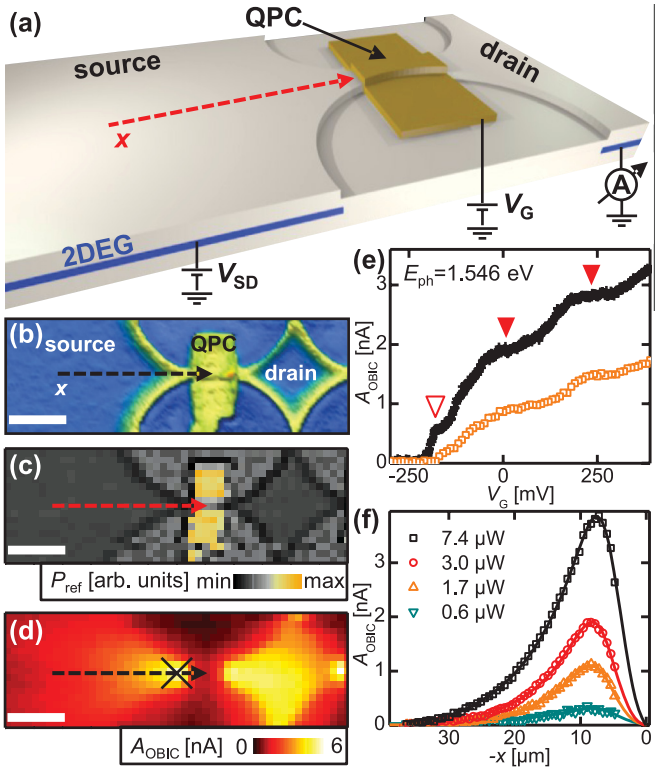

FIG. 1. (Color online) (a) Schematic image of a QPC with a golden opaque topgate and a 2DEG acting as source and drain contacts. (b) White light interferometric image of the sample. (c) Spatially resolved reflectance of the laser. (d) OBIC map of the circuit in (c) when left (right) 2DEG section acts as source (drain) contact ($V_G = 600$ mV, $V_{SD} = -2$ mV, $P_{laser} = 1$ μW, $E_{ph} = 1.598$ eV). (e) OBIC amplitude at position marked with a cross in (d) as a function of V_G for two different laser intensities $P_{laser} = 0.54$ μW (black crosses) and $P_{laser} = 0.22$ μW (orange open squares) ($V_{SD} = -2.5$ mV, $E_{ph} = 1.546$ eV). Several quantization steps of A_{OBIC} can be seen (triangles). (f) Dependence of A_{OBIC} (scattered points) on the distance of the excitation spot to the QPC [recorded along the dashed lines in (a), (b), (c), and (d)] for different P_{laser} ($V_G = 225$ mV, $V_{SD} = -2.5$ mV, $E_{ph} = 1.546$ eV). The data are fitted by Eq. (1). All measurements are performed at $T = 4.2$ K and $f_{trigger} = 40$ MHz. Scale bars in (b), (c), and (d) are 10 μm.

of the QPC, our OBIC spectroscopy is especially sensitive to changes of the chemical potential in the drain contact. In other words, when the laser is focused on the source side of the QPC, only those hot photogenerated electrons are predominantly detected which propagate through the QPC to the drain contact.[23] Focusing the laser on the drain side, the OBIC is also dominated by photoconductive gain effects, which are induced, for example, by the spatial separation of the photogenerated electrons and holes at the edge of the mesa.[29] At low laser intensities, the interband recombination of photogenerated electrons and holes can be neglected to describe the experimental photocurrent results. In a simplified picture, then, the overwhelming part of photogenerated holes are spatially localized close to the QPC and therefore, slightly separated from the area of the 2DEG. Only at high intensities, both charge-carrier clouds start to significantly overlap in space, and interband recombination processes need to be considered.

The integrated laser intensity is automatically adjusted by a motorized filter wheel in the power range from 100 nW to 100 μW on the chip. In addition, the intensity of the laser light reflected back from the sample P_{ref} is detected concurrently with A_{OBIC} as a function of the laser position. In combination with white light interferometric images [Fig. 1(b)] such reflectance scans [Fig. 1(c)] serve as orientation maps for the spatially resolved OBIC maps [Fig. 1(d)]. Keeping the laser focused on a fixed position at the source contact [cross in Fig. 1(d)], A_{OBIC} exhibits steps as a function of V_{G} [filled triangles in Fig. 1(e) for $P_{\mathrm{laser}} = 1$ μW] accounting for the one-dimensional subbands of the QPC.[21–23] In particular, these subbands are tuned by V_{G} in energy with respect to the chemical potentials in the source and drain leads. If not indicated elsewhere, all results presented are taken at the OBIC plateau at $V_{\mathrm{G}} = 225$ mV. For all laser intensities shown here, this voltage always corresponds to the second one-dimensional subband of the QPC, independent of the photoconductive gain effect caused by the photogenerated holes. This can be understood by the second A_{OBIC} trace for $P_{\mathrm{laser}} = 220$ nW [open squares in Fig. 1(e)]. Due to the reduced laser intensity, less photogenerated holes are accumulated in the region of the QPC, and in turn, the reduced photoconductive gain effect shifts the A_{OBIC} trace to more positive gate voltages.[26] But still, the second plateau can be detected at $V_{\mathrm{G}} = 225$ mV. The open triangle in Fig. 1(e) denotes a resonance which we interpret to origin either from an interference effect or an impurity in the vicinity of the QPC, which is beyond the scope of the present paper.[30–32]

Figure 1(f) shows typical cuts through OBIC maps vs the distance to the QPC [indicated as a dashed line in Fig. 1(d)] for different laser intensities. The scattered data points are fitted with a single-exponential decay with decay length δ_{decay} starting at the maximum amplitude $A^{\mathrm{max}}_{\mathrm{OBIC}}$ of the signal convoluted with a Gaussian profile with FWHM of σ_{c} representing the laser spot width. The fitting function reads

$$f(|x|) = A^{\mathrm{max}}_{\mathrm{OBIC}} e^{-\frac{|x|}{\delta_{\mathrm{decay}}}} * \frac{1}{\sqrt{2\pi}\sigma_{\mathrm{c}}} e^{-\frac{|x|^2}{2\sigma_{\mathrm{c}}^2}}. \qquad (1)$$

The fits are drawn as lines in Fig. 1(f). We note again that in the utilized OBIC spectroscopy at 40 MHz, A_{OBIC} in Fig. 1(f) represents photoexcitation events in the source contact which give rise to a change of the chemical potential in the drain region.[23] In other words, A_{OBIC} represents photogenerated electrons which propagate from source to drain, and δ_{decay} gives access to the average propagation length of the photogenerated hot electron ensemble in the source contact with the QPC acting as an energy filter. This propagation length as a function of the photon energy and the laser intensity is investigated in the present paper.

III. RESULTS

Figures 2(a) and 2(b) show an evaluation of the fitting parameter δ_{decay} of Eq. (1) as a function of the laser excitation intensity P_{laser} and the electronic excess energy ΔE. The decay length δ_{decay} shows a nonmonotonic dependence on P_{laser}. This can be seen in Fig. 2 for (a) quasiresonant excitation with $E_{\mathrm{ph}} = 1.546$ eV and (b) nonresonant excitation with $E_{\mathrm{ph}} = 1.598$ eV.

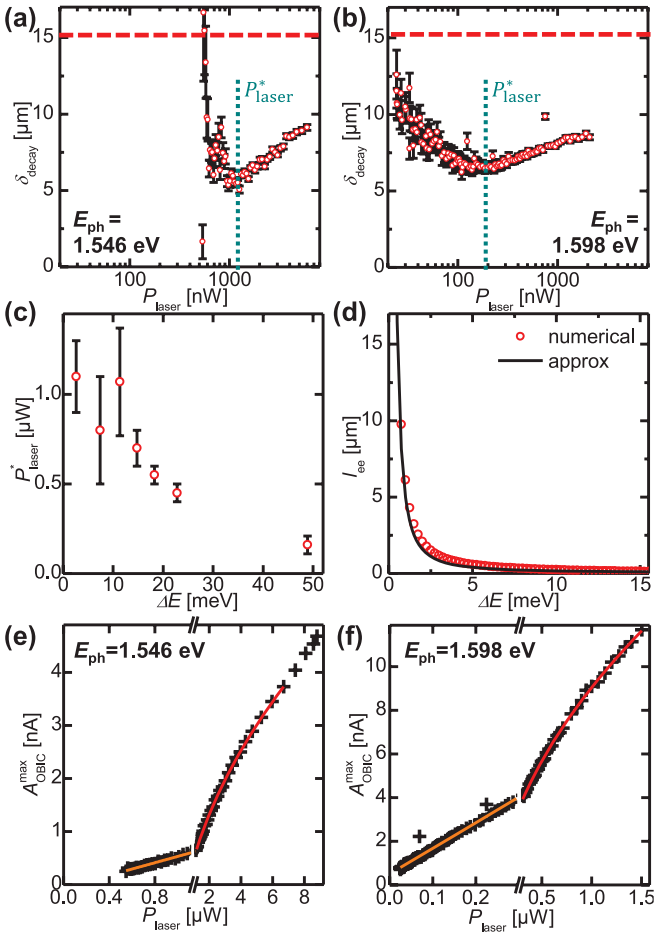

FIG. 2. (Color online) (a) and (b) The decay length δ_{decay} varies for all photon energies 1.546 eV $< E_{\mathrm{ph}} <$ 1.598 eV nonmonotonically with P_{laser} ($V_{\mathrm{SD}} = -2.5$ mV, $V_{\mathrm{G}} = 225$ mV). The dashed red line in both plots denotes the elastic mean free path $l_{\mathrm{mfp}} = 15.1$ μm in the 2DEG. The position of the minimum of δ_{decay} (P_{laser}) is denoted as P^*_{laser}. (c) P^*_{laser} as a function of excess energy ΔE. For higher photon energies, the transition occurs at lower values. (d) Theoretical calculation of the electron-electron scattering length according to Ref. 2. (e) and (f) Maximum OBIC amplitude $A^{\mathrm{max}}_{\mathrm{OBIC}}$ for two different photon energies. The lines show linear (square root) fits to the data for the low (high) laser power regime $P^*_{\mathrm{laser}} > P_{\mathrm{laser}}$ ($P^*_{\mathrm{laser}} < P_{\mathrm{laser}}$).

In particular, for the lowest laser powers and quasiresonant excitation, δ_{decay} is comparable to the elastic mean free path $l_{\mathrm{mfp}} = 15.1$ μm of the 2DEG [dashed lines in Figs. 2(a) and 2(b)]. For an increasing laser power, δ_{decay} gradually drops to a minimum value at a characteristic transition laser power denoted as $P^*_{\mathrm{laser}}(\Delta E)$. In Fig. 2(c), P^*_{laser} is plotted as a function of ΔE. We observe that the minimum of δ_{decay} always has a value of $5-7$ μm independent of ΔE, and it occurs at a decreasing laser power for increasing excess energies. For $P_{\mathrm{laser}} > P^*_{\mathrm{laser}}$, the propagation length gradually increases again [Figs. 2(a) and 2(b)], but it stays below l_{mfp} also for the highest laser intensities. We note that the qualitative behavior of δ_{decay} is the same for all excess energies ΔE and, most importantly, it does not change significantly when the excess energy is higher than 21 meV, where one would expect interaction effects with plasmons[2] and/or the second subband of the quantum well,[33,34]

and for ΔE larger than 35 meV, where longitudinal optical phonons can be emitted.[35,36]

Figure 2(d) shows a theoretical calculation of the electron-electron scattering length l_{ee} vs ΔE according to Giuliani *et al.*[2] The scattered red circles denote a numerical solution to Eq. (8) from Ref. 2 for zero temperature, whereas the solid black line depicts the approximation for low excess energies [Eq. (13) from Ref. 2]. This length scale is defined via the lifetime of a single particle excitation τ_{ee} as $l_{ee} = v_F \tau_{ee}$ and it denotes the length between individual scattering processes. Therefore, it is very different from the definition of the elastic mean free path l_{mfp}, which describes the average length scale along which an electron ensemble can propagate without inelastic scattering, that is, without the transfer of momentum out of the electronic system.

As we discuss in detail below, Figs. 2(e) and 2(f) show the fitting parameter A_{OBIC}^{max} for (e) quasiresonant ($E_{ph} = 1.546$ eV) and (f) nonresonant excitation ($E_{ph} = 1.598$ eV). For all photon energies we find two distinct characteristics for A_{OBIC}^{max} as a function of P_{laser}. For $P_{laser} < P_{laser}^{*}$, A_{OBIC}^{max} depends linearly on P_{laser}, while for $P_{laser} > P_{laser}^{*}$, A_{OBIC}^{max} is proportional to $\sqrt{P_{laser}}$. The lines are linear (square root) fits to the data for low (high) laser intensities, respectively.

The experimental data in Fig. 2 are all taken with the QPC tuned to the very broad and stable second quantization plateau. This allows us to change the laser power without adjusting the gate voltage, as would be necessary for the first quantization plateau. This, in turn, would capacitively influence the electron density around the QPC and possibly alter the scattering processes. Nevertheless, we see a very similar, nonmonotonical behavior of δ_{decay} for the first quantization plateau. We also find $A_{OBIC} \propto P_{laser}$ ($A_{OBIC} \propto \sqrt{P_{laser}}$) for $P_{laser} < P_{laser}^{*}$ ($P_{laser} > P_{laser}^{*}$) (data not shown). In these measurements, however, we had to adjust V_G, depending on the laser power, which makes the data less reliable than in the second plateau.

Further insight into the underlying electron dynamics is provided by additionally varying the source drain bias. In Fig. 3 we show A_{OBIC} measured at the position marked with a cross in Fig. 1(d) as a function of both V_{SD} and V_G for $E_{ph} = 1.546$ eV and $P_{laser} = 2.5\ \mu$W in (a) and $E_{ph} = 1.598$ eV and $P_{laser} = 9.4\ \mu$W in (b). Figure 3(c) depicts the dependence of A_{OBIC} as a function of V_{SD} for three different laser intensities, always at the onset of the first quantization plateau, as exemplarily indicated by the dashed black line in Fig. 3(a) (squares: $P_{laser} = 3.9\ \mu$W and $V_G = -200$ mV, circles: $P_{laser} = 2.3\ \mu$W and $V_G = -160$ mV, triangles: $P_{laser} = 0.6\ \mu$W and $V_G = 0$ V).[37] As already examined in detail in Ref. 23, we detect a signal asymmetric in bias voltage V_{SD}. At negative V_{SD}, the dominant contribution is due to the ballistic photocurrent, whereas at positive V_{SD} we see either a capacitive cross coupling, a reminiscent photoconductive gain effect, or a signal due to electrons that are excited at such high energies that they overcome the energetic barrier of the QPC. Therefore, at the first quantization plateau, where the QPC opens, the minimum of A_{OBIC} vs V_{SD} is a measure for the shift of the chemical potential in the source contact due to photogenerated electrons with respect to the drain contact. In Fig. 3(d) we evaluate the shift of the curves as in Fig. 3(c). The line is a square root fit to the data. We also find a quantitatively and qualitatively very

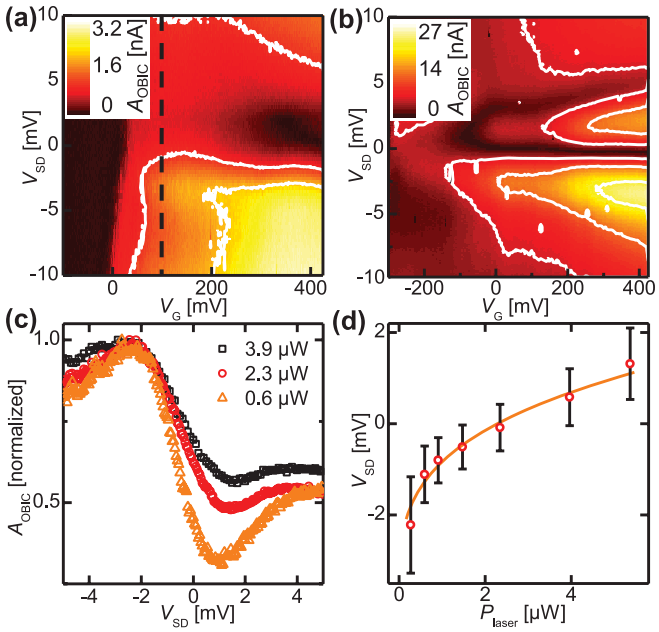

FIG. 3. (Color online) Dependence of OBIC amplitude A_{OBIC}^{max} on V_{SD} and V_G detected at the position marked with a cross in Fig. 1(d) for (a) $E_{ph} = 1.546$ eV and $P_{laser} = 2.5\ \mu$W and for (b) $E_{ph} = 1.598$ eV and $P_{laser} = 9.38\ \mu$W. (c) A_{OBIC} as a function of V_{SD} for three different laser intensities, at the onset of the first quantization plateau (squares: $P_{laser} = 3.9\ \mu$W and $V_G = -200$ mV, circles: $P_{laser} = 2.3\ \mu$W and $V_G = -160$ mV, triangles: $P_{laser} = 0.6\ \mu$W and $V_G = 0$ V) (d) Evaluation of the shift of the curves as in (c).

similar shift for QPC tuned to the second quantization plateau (data not shown). In this gate voltage regime, however, the position of the minimum of $A_{OBIC}(V_{SD})$ gets influenced by the increasing capacitive cross coupling at positive source drain biases. Therefore, it is more reliable to evaluate the relative position of the chemical potential at the onset of the first quantization plateau.

Figure 4(a) shows quantized OBIC curves for quasiresonant excitation with different laser intensities in a logarithmic scale ($V_{SD} = -2.5$ mV). Figure 4(b) depicts the pinch-off voltage of the current through the QPC as a function of laser power for

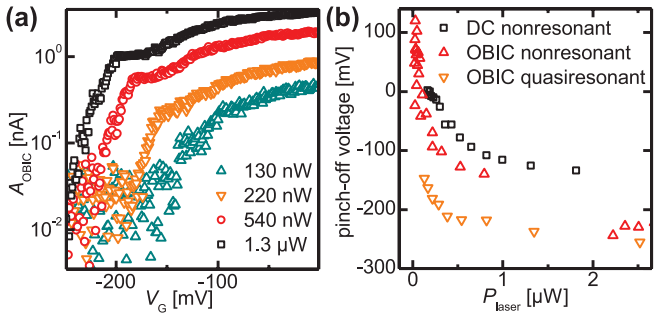

FIG. 4. (Color online) (a) Quantized A_{OBIC} vs V_g for different laser intensities ($E_{ph} = 1.546$ eV, $V_{SD} = -2.5$ mV). A shift of the pinch-off voltage with increasing power to lower V_g is clearly visible. (b) Pinch-off voltages of the OBIC curves as in (a) as a function of excitation intensity for different photon energies. See text for details.

both the transport conductance under laser irradiation (squares) as well as the photocurrent for quasiresonant (triangles with tip downwards) and nonresonant excitation (triangles with tip upwards). As can be seen, the shift saturates at laser powers above approximately 1 μW. We discuss the data in the following.

IV. DISCUSSION

There are several relaxation mechanisms with different time and length scales involved in the present experiment which we want to summarize before entering a detailed theoretical discussion. The hot photogenerated electrons can thermalize either via electron-electron scattering[19] or – for excess energies higher than 35 meV – via optical phonons.[14] Both mechanisms typically happen on time scales shorter than both the temporal FWHM of the laser of ∼142 ps and the average transit time for the photogenerated electrons to ballistically propagate from the laser excitation spot to the QPC, which is on the order of 66 ps $= l_{\mathrm{mfp}}/v_{\mathrm{F}}$. The experimentally determined thermalization time of a hot charge carrier ensemble in 3D bulk GaAs is on the order of 50 ps,[19,20] whereas relaxation via optical phonons usually happens within ∼1 ps.[14] According to Shah the relaxation rates in 2D systems with charge carrier densities of 10^{11} cm^{-2} are only slightly increased compared to the bulk values.[18] Typical quasiparticle lifetimes of an individual hot charge carrier lie on the order of $\tau_{\mathrm{ee}} \sim 1$ ps.[12] This corresponds to a length scale $l_{\mathrm{ee}} = \tau_{\mathrm{ee}} v_{\mathrm{F}} \approx 1\ \mathrm{ps} \cdot 2.3 \times 10^5\ \mathrm{m/s} = 230$ nm. l_{ee} is a single particle parameter and it is significantly shorter than the elastic electron mean free path for thermalized charge carriers $l_{\mathrm{mfp}} = 15.1\ \mu$m, which is an ensemble value. At low temperatures, l_{mfp} is mostly dominated by remote and background impurity scattering.[38–41]

Furthermore, the complete electron system including the photogenerated electrons is not a perfectly thermalized, degenerate Fermi gas. It is rather a combination of the originally present Fermi gas and a mixture of the initial Gaussian energy distribution of the photogenerated electrons. At time scales on the order of the transit time, the energy distribution of the photogenerated electrons can be assumed to be a Maxwell-Boltzmann distribution.[20]

The mesoscopic photocurrent dynamics are influenced by the following contributions: The enlarged scattering phase space due to a softened energy distribution, the screening of momentum scatterers, the formation of a quasi-Fermi level, and the eventual recombination of the photogenerated electrons and holes, as will be discussed in detail in the following sections.

V. IMPACT OF INCREASED SCATTERING PHASE SPACE

We consider the regime of the lowest laser intensities as a perturbative transport regime. Here only very few electrons are optically excited from the valence to the conduction band, compared to the number of electrons already present in the 2DEG due to doping. In this regime, we experimentally observe $\delta_{\mathrm{decay}} \approx l_{\mathrm{mfp}}$. Generally, the photogenerated electrons experience an enhanced electron-electron scattering compared to the completely thermalized 2DEG. The electron-electron quasiparticle lifetime τ_{ee} for a single hot electron excited with excess energy ΔE above a degenerate 2D Fermi gas is inversely proportional to $[\ln(\Delta E/E_{\mathrm{F}})]\,(\Delta E/E_{\mathrm{F}})^2$.[1,2] This is mainly due to the increased number of energetically available states in phase space when the excess energy is increased.[2] A detailed examination of the electron-electron scattering with electrons above the Fermi energy of a 2DEG with evaluation of the scattering lengths was done by Fasol.[3] We want to emphasize that, in contrast to our experiment, where we detect an average propagation length δ_{decay} of a photocurrent, $l_{\mathrm{ee}} = \tau_{\mathrm{ee}} v_{\mathrm{F}}$ describes the distance, which an individual electron propagates along a straight line until it is subject to an elastic electron-electron scattering event, which causes the direction of motion to be changed by a random angle.[4,7] In our experiment, the detection of individual photogenerated charge carriers is not possible. This particular scattering mechanism nevertheless nicely illustrates how the enlarged phase space increases the charge carrier interaction of photogenerated charge carriers. Analogously to the rapid decrease of the electron-electron scattering length as visualized in Fig. 2(d), we interpret the steep slope of our experimental curves in Figs. 2(a) and 2(b) to be mainly caused by the additionally available states caused by an addition of energy to the system. Beyond that, the nondegenerate Maxwell-Boltzmann distribution of the hot electron ensemble provides more available unoccupied energy states compared to a degenerate Fermi distribution. Consequently, we expect an even further enlarged phase space for scattering compared to purely degenerate systems. Due to the increased scattering rate, a certain fraction of the photogenerated electron ensemble can be scattered out of the beam and does not arrive at the QPC detector. This can either occur via a backscattering of a certain portion of electrons or via a deflection towards the not perfectly reflective boundaries. By this, we explain the significant decrease of the photocurrent propagation length δ_{decay} with increasing laser intensities in the low power regime [Figs. 2(a) and 2(b)].

VI. SCREENING EFFECTS

We interpret the increase of δ_{decay} for higher laser powers to be a footprint of both screening and scattering. On the one hand, the overall electron density n is increased because of the photogenerated electrons. Therefore both the background and remote impurities become more screened, and l_{mfp} increases.[39] Assuming a finally thermalized Fermi-Dirac energy distribution, the increased electron density leads to an increased Fermi energy

$$E_{\mathrm{F}} = \frac{\hbar^2 k_{\mathrm{F}}^2}{2m^*} = \frac{\hbar^2 \pi (n_0 + n_{\mathrm{opt}})}{m^*}, \tag{2}$$

with k_{F} the Fermi wave vector, m^* is the effective mass in GaAs, n_0 is the density of the initially present electrons, and n_{opt} is the density of the photogenerated electrons. We estimate the density of the photogenerated electrons within one pulse as follows:

$$\frac{n_{\mathrm{opt}}}{\mathrm{pulse}} = \frac{P_{\mathrm{laser}}}{E_{\mathrm{ph}} A f_{\mathrm{trigger}}} (1-R) e^{-\beta \cdot D} (1 - e^{-\alpha w}) = 2.5 \times 10^{10}\ \mathrm{cm}^{-2}. \tag{3}$$

Here we assume a laser power $P_{\text{laser}} = 1\ \mu\text{W}$, $E_{\text{ph}} = 1.546$ eV, $f_{\text{trigger}} = 40$ MHz, and a spot size A of $1.5^2\pi\ \mu\text{m}^2$. The second half of the formula considers the absorption and reflection coefficients of the heterostructure. The reflection coefficient is taken to be $R = 0.3$, the absorption of AlGaAs at the chosen wavelength $\beta = 0$ and the absorption of GaAs in the $w = 25$ nm wide quantum well to be $10^4\ \text{cm}^{-1}$. The calculated density of the photogenerated electrons would already increase the Fermi level by 900 μeV at a laser power of 1 μW, which is in accordance with our measurement in Fig. 3(d). Assuming a thermalized electron distribution, we thereby increase the Fermi energy and thus the electron density by approximately 10%−50%. Previous experiments showed an increase of the mobility μ with the two-dimensional charge carrier density n as $\mu \sim n^{\gamma}$ with $\gamma = 1.4$ and 1.2 for remote and background impurity, respectively.[39] This would result in an increase of a factor ∼1.5 in mobility for the used laser intensities. Assuming a constant velocity, this leads to an increase in the propagation length on the same order, which we see for all wavelengths for $P_{\text{laser}} > P^*_{\text{laser}}$ [Figs. 2(a) and 2(b)].

On the other hand, the Rutherford scattering cross section in the classical limit is inversely proportional to the total kinetic energy (not only excess energy) in two dimensions.[42,43] By this, both the single particle scattering time and the elastic momentum relaxation time are increased. Therefore, we interpret the transition laser power P^*_{laser} to characterize the relative influences of the scattering versus screening effects. For a higher ΔE of the photogenerated electrons, more energy and momentum is distributed within the electron ensemble during the thermalization process. Thus, the average kinetic energy per electron of the overall electron ensemble is higher, which in turn, shifts the curves δ_{decay} vs P_{laser} to a lower P_{laser} [compare Figs. 2(a) to 2(b), Fig. 2(c)].

VII. FORMATION OF A QUASI-FERMI LEVEL AND RECOMBINATION

From Fig. 3(d) we deduce that the chemical potential in the source contact is shifted due to the addition of photogenerated electrons by $\leqslant 3$ meV for all examined P_{laser}. In the following we consider the dependence of the quasistatic number of photogenerated electrons on the laser excitation intensity. This, in turn, strongly depends on the number of holes that accumulate in the vicinity of the QPC. The rate equation, which describes the number of photogenerated electrons around the laser spot in a quasistatic balance, can be written as follows:

$$\dot{n}_{\text{opt}} = c_1 P_{\text{laser}} - c_2 n_{\text{opt}} - c_3 n_{\text{opt}} n_{\text{opt}} \equiv 0, \tag{4}$$

with the proportionality constant c_1 describing the generation mechanism. The formula further considers the change due to the photocurrent, which is proportional to the number of electrons ($c_2 n_{\text{opt}}$), and the recombination with a proportionality constant c_3. The recombination is proportional to the number of electrons n_{opt} and the number of holes, which in a first approximation also equals n_{opt}, as the charge carriers are generated as electron-hole pairs.

For low excitation intensities, the number of photogenerated electron-hole pairs is smaller than the available states for photogenerated holes in the vicinity of the QPC below the opaque topgate. Thus, the photogenerated electrons and holes can be eventually spatially separated by a few micrometers, and the recombination rate c_3 is greatly suppressed. Then, Eq. (4) simplifies to

$$\dot{n}_{\text{opt}} = c_1 P_{\text{laser}} - c_2 n_{\text{opt}} \equiv 0. \tag{5}$$

In this case, the number of electrons n_{opt} that contribute to the OBIC current is directly proportional to P_{laser} and both the new quasi-Fermi level $E_{\text{F}} = \frac{\hbar^2 k_{\text{F}}^2}{2m^*} = \frac{\hbar^2 \pi n}{m^*}$ and $A_{\text{OBIC}} \propto n_{\text{opt}}$ should increase linearly with P_{laser}. We cannot resolve the quasi-Fermi level for such a low P_{laser}. However, A_{OBIC} in Figs. 2(e) and 2(f) clearly increases linearly with excitation intensity in the low power regime, as expected from Eq. (5).

For sufficiently high excitation intensities, all states for photogenerated holes are finally occupied in the vicinity of the QPC. We verify this scenario by measuring the saturation of the photoconductive gain effect above $P_{\text{laser}} \sim 1\ \mu\text{W}$ [Fig. 4(b)]. In this intensity regime, more and more photogenerated holes are not diffusing and drifting to the position of the QPC but stay in the source region. This enhances the influence of the recombination of the photogenerated electrons with holes as a relaxation path for increasing P_{laser}. Typical recombination times for 2D electron-hole plasmas in GaAs lie on the order of 400 ps.[44] Due to this additional relaxation path for the photogenerated electrons, the number of free photogenerated electrons n_{opt} follows a square root dependence, as becomes evident when solving Eq. (4) in the quasistatic case for a non-negligible recombination rate c_3. Consecutively, this explains the square root dependence of the optically induced quasi-Fermi level [Fig. 3(d)] and in turn A_{OBIC} [Figs. 2(e) and 2(f)].

VIII. DISCUSSION OF THERMOELECTRIC EFFECTS

Molenkamp *et al.* investigated thermoelectric effects using a beam of hot electrons to heat up a 2DEG.[9,11] They found a quadratic dependence of the dissipated energy with their heating current, which they could explain by Joule heating. The thermoelectric treatment of the electron-electron interaction was consecutively expanded to a hydrodynamic analog which dominates the transport properties in narrow conducting regions.[45,46] Under certain experimental conditions, electron-electron scattering can lead to a nonmonotonic energy dependence of the number of electrons scattered out of an electron distribution.[8] This effect was attributed to a crossover from the ballistic to the hydrodynamic regime of electron flow, which again could in principle be similar in our experiment. However, such a model cannot explain our data as becomes evident by the following argument. The thermopower, quantified by the Seebeck coefficient S, of a single QPC describes the shift of the chemical potential due to a temperature difference. It was measured by van Houten *et al.* to be $S = -20\ \mu\text{V/K}$.[10] To get a shift on the order of 1 meV [Fig. 3(d)], this would require a temperature difference of 50 K between the source and drain contacts. Such an assumed temperature is in contradiction to the fact, that we still detect very pronounced steps in A_{OBIC} for all examined P_{laser} [e.g., Fig. 1(e)]. The subband spacing is 4 meV, and we typically do not detect the one-dimensional subbands in our optoelectronic experiment above ∼17 K.[47] Instead, we explain the characteristic square root dependence

of our data by the existence of a photogenerated quasi-Fermi level at high laser intensities.

IX. CONCLUSIONS

In summary, we present spatially resolved photocurrent measurements in a 2DEG using a QPC as local photocurrent detector. We extract the propagation length of the photogenerated electron ensemble and identify three different regimes depending on the excitation intensities. For low excitation intensities, the electronic system is only slightly perturbed and the propagation length of the photogenerated electron ensemble is comparable to the elastic mean free path extracted from transport measurements. With increasing laser intensity, an enlarged phase space with more available states increases scattering and reduces the propagation length. For the largest excitation intensities, the photocurrent propagation length increases again which we interpret to be caused by an enhanced screening of momentum scatterers at an overall enlarged electron density with an optically induced quasi-Fermi level.

ACKNOWLEDGMENTS

We thank G. Abstreiter and A. Högele for technical support and we thank J. P. Kotthaus, A. V. Chaplik, D. Taubert, and G. J. Schinner for fruitful discussions. Financial support from the German Science Foundation DFG (Ho 3324/4), the Center for NanoScience (CeNS), and the German excellence initiative via the "Nanosystems Initiative Munich (NIM)" is gratefully acknowledged. M. Stallhofer gratefully acknowledges the support of the TUM Graduate School's Faculty Graduate Center of Physics at the Technische Universität München.

*Corresponding author: holleitner@wsi.tum.de

[1] A. V. Chaplik, Zh. Eksp. Teor. Fiz. **60**, 1845 (1971) [Sov. Phys. **33**, 997 (1971)].
[2] G. F. Giuliani and J. J. Quinn, Phys. Rev. B **26**, 4421 (1982).
[3] G. Fasol, Appl. Phys. Lett. **59**, 2430 (1991).
[4] D. R. S. Cumming and J. H. Davies, Appl. Phys. Lett. **69**, 3363 (1996).
[5] L. Zheng and S. Das Sarma, Phys. Rev. B **53**, 9964 (1996).
[6] H. Predel, H. Buhmann, L. W. Molenkamp, R. N. Gurzhi, A. N. Kalinenko, A. I. Kopeliovich, and A. V. Yanovsky, Phys. Rev. B **62**, 2057 (2000).
[7] A. V. Yanovsky, H. Predel, H. Buhmann, R. N. Gurzhi, A. N. Kalinenko, A. I. Kopeliovich, and L. W. Molenkamp, Europhys. Lett. **56**, 709 (2001).
[8] R. N. Gurzhi, A. I. Kopeliovich, A. N. Kalinenko, A. V. Yanovsky, E. N. Bogachek, U. Landman, H. Buhmann, and L. W. Molenkamp, Phys. Rev. B **68**, 165318 (2003).
[9] L. W. Molenkamp, H. van Houten, C. W. J. Beenakker, R. Eppenga, and C. T. Foxon, Phys. Rev. Lett. **65**, 1052 (1990).
[10] H. van Houten, L. W. Molenkamp, C. W. J. Beenakker, and C. T. Foxon, Semicond. Sci. Technol. **7**, B215 (1992).
[11] L. W. Molenkamp, M. J. P. Brugmans, H. van Houten, and C. T. Foxon, Semicond. Sci. Technol. **7**, B228 (1992).
[12] T. Schäpers, M. Krüger, J. Appenzeller, A. Förster, B. Lengeler, and H. Lüth, Appl. Phys. Lett. **66**, 3603 (1995).
[13] G. J. Schinner, H. P. Tranitz, W. Wegscheider, J. P. Kotthaus, and S. Ludwig, Phys. Rev. Lett. **102**, 186801 (2009).
[14] D. Taubert, C. Tomaras, G. J. Schinner, H. P. Tranitz, W. Wegscheider, S. Kehrein, and S. Ludwig, Phys. Rev. B **83**, 235404 (2011).
[15] M. A. Topinka, B. J. LeRoy, S. E. J. Shaw, E. J. Heller, R. M. Westervelt, K. D. Maranowski, and A. C. Gossard, Science **289**, 2323 (2000)
[16] M. A. Topinka, B. J. LeRoy, R. M. Westervelt, S. E. J. Shaw, R. Fleischmann, E. J. Heller, K. D. Maranowski, and A. C. Gossard, Nature (London) **410**, 183 (2001).
[17] M. P. Jura, M. Grobis, M. A. Topinka, L. N. Pfeiffer, K. W. West, and D. Goldhaber-Gordon, Phys. Rev. B **82**, 155328 (2010).
[18] J. Shah, *Ultrafast Spectroscopy of Semiconductors and Semiconductor Nanostructures*, 2nd ed., Springer Series in Solid-State Sciences (Springer, Berlin, 1999).
[19] D. W. Snoke, W. W. Rühle, Y.-C. Lu, and E. Bauser, Phys. Rev. B **45**, 10979 (1992).
[20] D. W. Snoke, W. W. Rühle, Y.-C. Lu, and E. Bauser, Phys. Rev. Lett. **68**, 990 (1992).
[21] B. J. vanWees, H. van Houten, C. W. J. Beenakker, J. G. Williamson, L. P. Kouwenhoven, D. van der Marel, and C. T. Foxon, Phys. Rev. Lett. **60**, 848 (1988).
[22] D. A. Wharam, T. J. Thornton, R. Newbury, M. Pepper, H. Ahmed, J. E. F. Frost, D. Hasko, D. C. Peacock, D. A. Ritchie, and G. A. C. Jones, J. Phys. C **21**, L209 (1988).
[23] K.-D. Hof, F. J. Kaiser, M. Stallhofer, D. Schuh, W. Wegscheider, P. Hänggi, S. Kohler, J. P. Kotthaus, and A. W. Holleitner, Nano Lett. **10**, 3836 (2010).
[24] T. Wilson, J. N. Gannaway, and P. Johnson, J. Microsc. **118**, 309 (1980).
[25] K.-D. Hof, C. Rossler, W. Wegscheider, S. Ludwig, and A. W. Holleitner, Phys. E **40**, 1739 (2008).
[26] K.-D. Hof, C. Rossler, S. Manus, J. P. Kotthaus, A. W. Holleitner, D. Schuh, and W. Wegscheider, Phys. Rev. B **78**, 115325 (2008).
[27] S. S. Buchholz, S. F. Fischer, U. Kunze, D. Reuter, and A. D. Wieck, Appl. Phys. Lett. **94**, 022107 (2009).
[28] S. F. Fischer, G. Apetrii, U. Kunze, D. Schuh, and G. Abstreiter, Nat. Phys. **2**, 91 (2006).
[29] C. Rössler, K.-D. Hof, S. Manus, S. Ludwig, J. P. Kotthaus, J. Simon, A. W. Holleitner, D. Schuh, and W. Wegscheider, Appl. Phys. Lett. **93**, 071107 (2008).
[30] A. Szafer and A. D. Stone, Phys. Rev. Lett. **62**, 300 (1989).
[31] M. P. Jura, M. A. Topinka, L. Urban, A. Yazdani, H. Shtrikman, L. N. Pfeiffer, K. W. West, and D. Goldhaber-Gordon, Nat. Phys. **3**, 841 (2007).
[32] D. Többen, D. A. Wharam, G. Abstreiter, J. P. Kotthaus, and F. Schäffler, Phys. Rev. B **52**, 4704 (1995).
[33] H. L. Störmer, A. C. Gossard, and W. Wiegmann, Solid State Commun. **41**, 707 (1982).

[34]B. Laikhtman, U. Sivan, A. Yacoby, C. P. Umbach, M. Heiblum, J. A. Kash, and H. Shtrikman, Phys. Rev. Lett. **65**, 2181 (1990).

[35]U. Sivan, M. Heiblum, and C. P. Umbach, Phys. Rev. Lett. **63**, 992 (1989).

[36]We note that measurements on another sample of the same heterostructure revealed a qualitatively similar result, although with higher absolute values for δ_{decay}.[23] We explain the difference by the use of a mode-locked pulsed nonresonant laser with a broader energetic width of 12 meV. The latter possibly excites electrons to the second subband.[34]

[37]The position of the first quantization plateau in Fig. 3(c) is shifted to more negative gate voltages as in Fig. 3(a) ($V_{\mathrm{G}} = -200$ mV as compared to $V_{\mathrm{G}} \sim 100$ mV). This is due to a different electrostatic environment as the sample was warmed up to room temperature and cooled down again to $T = 4.2$ K between the two measurements.

[38]R. Dingle, H. L. Störmer, A. C. Gossard, and W. Wiegmann, Appl. Phys. Lett. **33**, 665 (1978).

[39]W. Walukiewicz, H. E. Ruda, J. Lagowski, and H. C. Gatos, Phys. Rev. B **30**, 4571 (1984).

[40]H. L. Störmer, Surf. Sci. **132**, 519 (1983).

[41]S. Hiyamizu, J. Saito, K. Nanbu, and T. Ishikawa, Jpn. J. Appl. Phys. **22**, 609 (1983).

[42]T. Ando, A. Fowler, and F. Stern, Rev. Mod. Phys. **54**, 437 (1982).

[43]F. Stern and W. E. Howard, Phys. Rev. **163**, 816 (1967).

[44]F. Daiminger, B. Neppert, A. Forchel, and J. Straka, Phys. Status Solidi **173**, 397 (1992).

[45]M. J. M. de Jong and L. W. Molenkamp, Phys. Rev. B **51**, 13389 (1995).

[46]L. W. Molenkamp and M. J. M. de Jong, Phys. Rev. B **49**, 5038 (1994).

[47]K.-D. Hof, C. Rössler, S. Manus, J. P. Kotthaus, D. Schuh, W. Wegscheider, and A. W. Holleitner, AIP Conf. Proc. **1199**, 331 (2010).